CERN Summer Student Programme 2024

EP-DT-DD SSD Group

REPORT

CHARACTERIZATION AND IRRADIATION STUDIES OF n-LGADS

Margarita Biveinytė

Vilnius University, Vilnius, Lithuania

Supervisors:

Veronika Kraus

CERN, Organisation europénne pour la recherche nucléaire, Geneva, Switzerland

Technische Universität Wien, Vienna, Austria

Moritz Wiehe

CERN, Organisation europénne pour la recherche nucléaire, Geneva, Switzerland

SSD group leader: **Michael Moll**

CERN, Organisation europénne pour la recherche nucléaire, Geneva, Switzerland

Geneva 2024

ABSTRACT

Over the past few years, Low Gain Avalanche Detectors (LGADs) have shown outstanding performance in detecting high-energy particles and they are the selected technology for the timing detectors of the upcoming ATLAS and CMS upgrade of the High-Luminosity Large Hadron Collider (HL-LHC). Although they suffer from radiation damage, they demonstrate good timing resolution and signal-to-noise (S/N) ratio due to the avalanche multiplication mechanism in the gain layer. As the charge multiplication mechanism is different for electrons and holes, the detection performance for low penetrating particles in p-type LGADs is reduced. By exchanging the conductivity type of all layers in an LGAD, n-type LGAD is obtained. The novel concept of n-LGAD detector from *Centro Nacional de Microelectronica* (IBM-CNM, Spain) could be relevant for detecting low penetrating particles, such as low energy particles and soft X-rays. Even though the intended field of application for n-LGADs lies outside of Hight Energy Physics (HEP), it still can be relevant for HEP R&D to investigate the fundamental material properties and compare to the p-type LGAD concept.

In this work, capacitance-voltage (C-V), current-voltage (I-V) as well as Transient Current Technique (TCT) and edge-TCT measurements were performed for n-type LGADs and PiNs (with and without window opening on metal) manufactured by IMB-CNM and irradiated with 23 GeV protons of different fluences: high fluences up to Φ = 2.5×10^{15} p/cm^2 for samples without a window opening on metal and step-by-step irradiation of one device up to Φ = 1×10^{13} p/cm^2 for samples with a window opening on metal.

ACKNOWLEDGMENT

I would like to express my deepest and most heartfelt gratitude to my esteemed supervisors, Veronika Kraus and Moritz Wiehe. Your unwavering kindness, exceptional guidance, and steadfast support have been the cornerstone of this project. Your insightful feedback, coupled with your patience and encouragement, has not only shaped this work but also enriched my understanding, inspiring me to reach new heights.

I am profoundly thankful to the remarkable members of the SSD group: Michael Moll, Marcos Fernandez Garcia, Yana Gurimskaya, Ruddy Costanzi, Leo Cavazzini, Faiza Rizwan and Niels Sorgenfrei. Your warm hospitality and unwavering support during my stay at CERN created an environment of collaboration and friendship that was both productive and deeply fulfilling. The sense of community you provided was invaluable.

Furthermore, I extend my sincerest thanks to Giuseppe Pezzullo at PS-IRRAD, CERN, for his assistance in irradiating the sensors and for the enlightening tour of the IRRAD facility. Your expertise and willingness to share your knowledge made a significant impact on this work.

CONTENTS

1 INTRODUCTION

1.1 Silicon sensors

Silicon is the most widely used semiconductor in micro- and nano-electronics applications due to its high availability and comparably small bandgap (1.12 eV at room temperature). Silicon-based particle sensors (*Fig. 1*) are widely employed in high-energy and nuclear physics experiments for tracking particles and radiation registering because of their good spatial and timing resolution and the possibility to produce them at commercial vendors in large quantities.

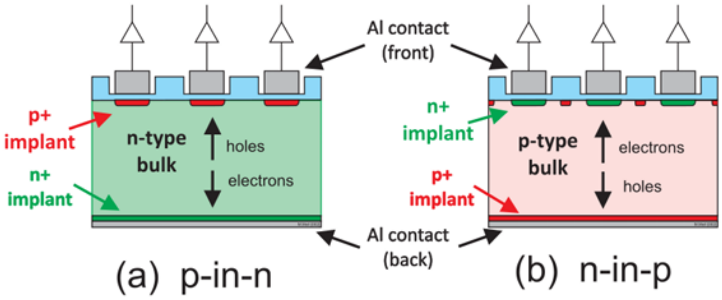

Fig. 1.: Silicon sensors in HEP. Schematic cross-section of a segmented n-type (a) and p-type (b) silicon detector [1].

Silicon sensors' working principle is based on p-n junctions at reverse bias. High-energy particles ionize silicon atoms and creates electron-hole pairs that are collected by the electrodes while using bias voltage to deplete the detector. This creates an electric field in which the charges can reach the electrodes. Collected charge is converted into an electrical signal to determine the particle's properties.

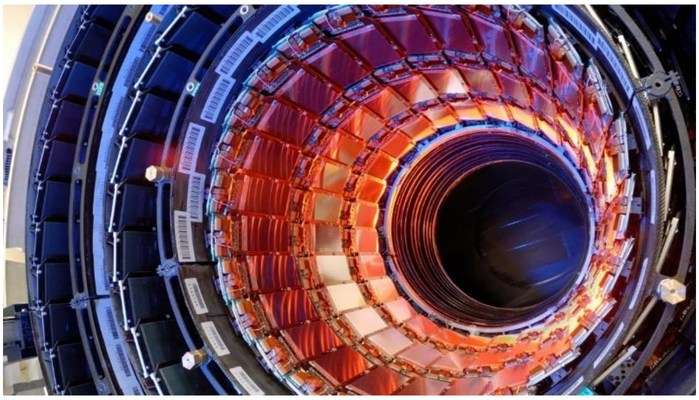

Fig. 2.: Example for the utilization of silicon sensors in CMS Inner Tracker [1].

However, in high-energy physics silicon sensors must withstand an intense radiation environment (*Fig. 2*), which creates a unique challenge for the design and operation of these sensors. High-energy radiation creates electrically active defects within the bandgap of the material, which determine the deterioration of silicon sensors' functional characteristics such as increase of leakage current, decrease of charge collection efficiency and degradation of timing resolution.

1.2 RADIATION DAMAGE

Since after the LHC upgrades semiconductor detectors will face >10^{16} n_{eq}/cm^2 (HL-LHC) and >7×10^{17} n_{eq}/cm^2 (FCC-hh) radiation dose. Therefore, it is very important to develop new radiation hardened structures, investigate new technologies and improve existing ones, as current detectors used at LHC cannot be operated after such irradiation [2]. Some examples for new detector technologies are LGADs, HV-CMOS, 3D Hybrid Pixel Detectors, etc., which need to be evaluated and optimized in terms of radiation hardness and/or 4D tracking capabilities.

The main effects of radiation damage:

• **Ionizing Energy Loss** (surface effect): trapping charges in the oxide, main effect for electronics).

• **Non Ionizing Energy Loss** (bulk effect): silicon atoms displaced from the lattice position, interstitials and vacancies formed – Frenkel pairs, resulting in point and cluster defects).

• **Creation of defect states in the band gap** (*Fig. 3*), which change internal electric field (charged defects change depletion, leading to under depletion and loss of signal), causes charge trapping (loss of signal charge) and increase of leakage current (increase of power consumption and noise).

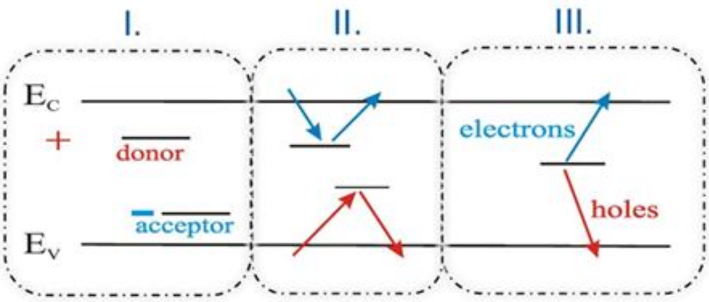

Fig. 3.: Creation of defects states in the band gap – change of internal electric field (I), charge trapping (II), increase of leakage current (III) [1].

The bulk damage produced in silicon particle detectors by high-energy particles is caused primarily by displacing a primary knock-on atom out of its lattice site resulting in a silicon interstitial and a left-over vacancy (Frenkel pair). Both can migrate through the lattice and may form point defects with impurity atoms being resident in the silicon [3].

The leakage current (generation current or dark current) is produced by defect levels close to the middle of the bandgap and its increase leads to higher noise and increase of power consumption. As the leakage current depends on the temperature, cooling is a very effective way to reduce the detrimental effects [2]. The temperature dependence of the leakage current is dominated by the position of the energy levels in the band gap, their cross sections and concentrations. The most efficient generation centers are at the intrinsic energy level.

In undamaged sensors, the bulk doping (phosphorus or boron) forms the effective space charge. Radiation-induced changes to the effective space charge lead to a change of the electric field distribution in a device and shift the depletion voltage to lower or higher values. With irradiation, higher operation voltages need to be applied to establish an electric field throughout the full sensor volume to avoid underdepletion and loss of active volume and signal (if high voltage cannot be applied, sensors will be operated underdepleted with the corresponding loss in the signal) [2]. Inhomogeneous distribution of space charge might lead to double junction effects or the shift of the highest electric field toward regions that are unprofitable for segmented sensors. High local fields can lead to impact ionization effects or breakdown [2]. The change of the space charge in silicon is strongly material-dependent (e.g. oxygen content) and depending on the particle type used for the irradiation experiment (e.g. neutron/proton damage) [2].

Charge carriers generated by ionizing particles or photons are collected by electrodes and constitute the sensor signal. Defect levels can capture (trap) charge carriers, and if the detrapping time of the charge carriers is longer than the collection time of the system or if the concentration of defects (trapping centers) is very high, the overall signal of the sensor is reduced [2]. Trapping becomes the limiting factor for high-fluence applications. The collection of electrons instead of holes at the electrodes may be an advantage due to the higher mobility of electrons and the possibility to exploit charge multiplication by impact ionization in lower fields without device breakdown [2].

1.3 Low Gain Avalanche Detectors (LGADs)

The Low Gain Avalanche Detector (LGAD) is a semiconductor (silicon-based) detector with signal amplification (*Fig. 4*), where in a highly doped p^+ gain layer a high electric field is created which leads to avalanche multiplication of primary electrons through impact ionization. LGADs implemented as $n^{++}p^+p$ (*Fig. 5*) represent a promising technology for the future LHC upgrades and for 4D tracking applications due to their good timing performance (fast signal rise time and optimal signal-to-noise (S/N) ratio).

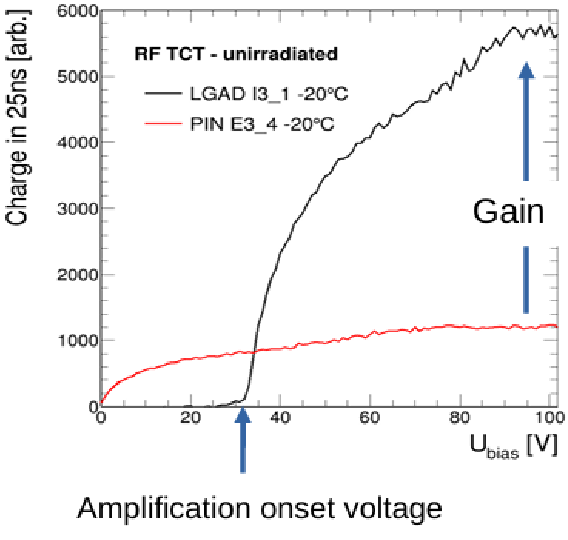

Fig. 4.: LGAD signal gain with respect to a standard PiN detector due to the avalanche multiplication [4].

Although LGADs show outstanding performance when detecting high-energy charged particles, they also suffer from radiation induced performance degradation, which causes the loss of signal gain because of acceptor removal in the gain layer.

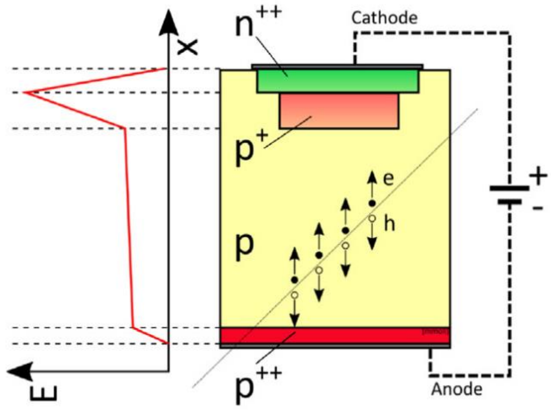

Fig. 5.: A schematic cross-section of a standard pad-like p-type LGAD [5].

Acceptor removal is the transformation of electrically active shallow acceptors into defect complexes because of the radiation for the all p-type devices. Boron, which is mostly used in p-type silicon production, is removed from the substitutional lattice site (B_s) and bound into defect complexes such as B_iO_i (Boron Interstitial-Oxygen interstitial) or B_sSi_i (Boron Substitutional-Silicon interstitial) which no longer exhibit shallow acceptor properties. The gain layer (p^+) is produced by a boron implantation that penetrates deeper into the silicon bulk than the shallow phosphorus implant (n^{++}) that constitutes the cathode of the device [6]. The negative space charge contributed by the shallow dopants is, therefore, lost and overall space charge is altered [6]. Experimentally, the removal process is, for example, characterized by the change in the gain layer depletion voltage of silicon sensors as a function of irradiation fluence.

1.4 THE NOVEL N-LGAD CONCEPT

By exchanging the conductivity type of all layers in an LGAD: electrodes, gain layer and bulk, we obtain the novel n-type LGAD (n-LGAD) (*Fig. 6*). The novel n-LGAD concept is optimized for low penetrating particles such as low energy protons and soft X-rays, due to the difference in multiplication mechanism for electrons and holes, where impact ionization rate is higher for electrons than for holes [5, 7].

In a traditional LGAD, a high-penetrating particle (IR light) has a higher gain response than a low-penetrating particle (UV light) due to the direction of the carrier drift: electrons are the major contributors to trigger the avalanche mechanism for IR light, while holes are for UV light, so the gain for IR light is higher than gain for UV light [5, 7]. For n-LGADs the situation is reversed: holes are the major contributor to trigger the avalanche mechanism for IR light, while electrons are for UV light, so the gain for IR light is smaller than for UV light [5, 7].

In n-type LGADs electrons and holes drift in opposite directions compared to a traditional LGAD. In n-type LGADs multiplication layer is diffused in between the p^{++} electrode and high resistivity n-type bulk, which generates a high electric field around the junction when the detector is reverse biased. Holes are drifting to the top of the sensor to the n^{+} gain layer, while the electrons are drifting to the bottom (n^{++}). In this case, for IR light there will be a greater number of holes crossing the high electric field region, so they will be the main carrier contributing to the avalanche mechanism triggering. For UV light, electrons are the major carrier that passes through the gain layer and therefore the concept exploits the beneficial impact ionization properties of electrons for low penetrating particles.

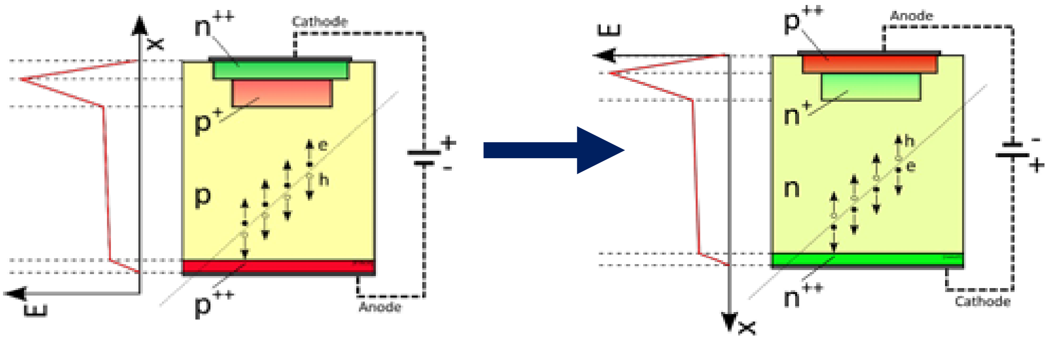

Fig. 6.: A schematic cross-section of a standard pad-like p-type LGAD (left) and the novel n-type LGAD with inverted conductivity types (right) [5].

It should be highlighted that described in the following report are the first ever radiation tests of such a structure. Even though the indented field of application for n-LGADs lies outside of HEP, it still can be relevant for HEP R&D to investigate the fundamental material properties and compare to the p-type LGAD concept. The SSD group at CERN, also within the scope of this Summer Student Project, is keen to investigate the fundamental device properties such as impact ionization and compare donor removal with irradiation in the n^{+} gain layer to the well-studied acceptor removal in p-type LGADs (see *section 1.3*). It also can be relevant to the compensated LGAD concept in High Energy Physics [8].

In the innovative design of compensated LGAD the purpose is to design a gain layer resulting from overlap of a p^{+} and n^{+} implants: the difference between acceptor and donor doping will result in an effective concentration of about 5×10^{16} cm^{-3}, similar to standard LGADs [8]. The new design might be more resilient to radiation, as both acceptor and donor atoms will undergo removal due to the higher doping at a slower rate, but the difference should remain constant, which is currently under investigation [8].

2 SAMPLES AND PROTON IRRADIATION

In this study single n-type LGADs (*Fig. 7*) and PiN diodes for a comparison, produced by IBM-CNM are investigated. There are two types of samples with different active areas: smaller samples with an active area 1.0×1.0 mm² without a window opening on the topside metallization (in *Table 1* marked as {1}, see *Fig. 8*) and bigger samples with an active area 1.3×1.3 mm² with a window opening on the topside metallization (in *Table 1* marked as {2}, see *Fig. 9*). All sensors are 275 µm thick with a resistivity of 30 kΩcm.

Fig. 7.: Photograph of n-LGAD sample produced by IBM-CNM studied in this work (top view of a device). The corresponding PiN sensors of the same producer look identical.

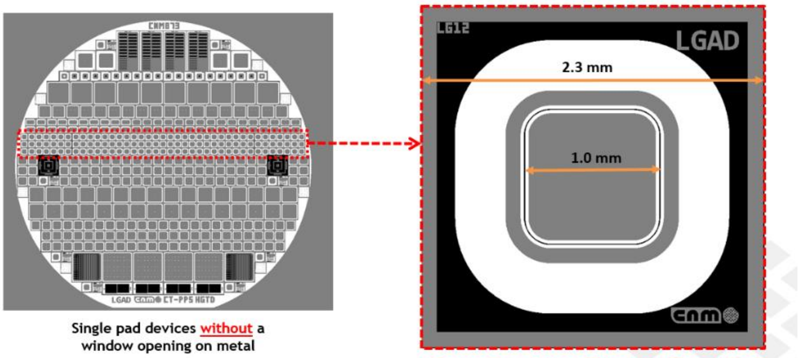

Fig. 8.: Sketch of the wafer layout of the CNM n-LGAD run R16375 without a window opening on metal (later named as "high fluence irradiation samples"). The corresponding PIN sensors of the same producer look identical [7].

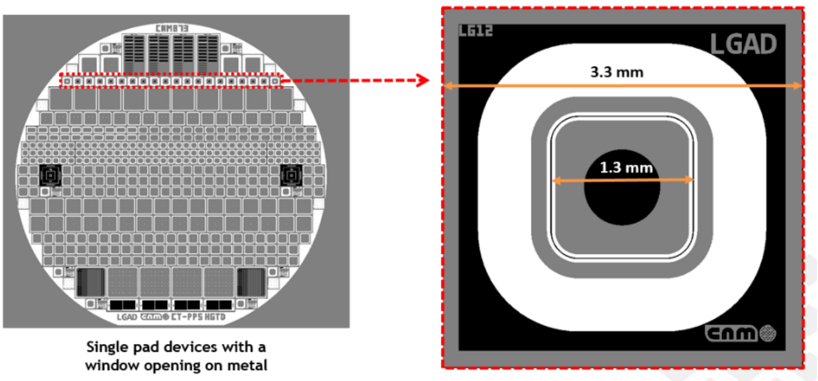

Fig. 9.: Sketch of the wafer layout of the CNM n-LGAD run R16375 with a window opening on metal (later named as "step-by-step irradiated samples"). The corresponding PIN sensors of the same producer look identical [7].

All samples were irradiated with protons of 23 GeV energy, hardness factor κ = 0.62. The first five samples (see *Table 1*) were irradiated with high fluences up to 2.5×10^{15} p/cm^2 (the same for n-PiN diodes for a comparison). In addition, one n-LGAD and one n-PiN sample were irradiated step-by-step up to 1×10^{13} p/cm^2. Samples were irradiated at the PS-IRRAD facility at CERN in SHUTTLE IRRAD-1 (see *Fig. 10*). The sensors were stored at -20°C after irradiation to prevent annealing.

Fig. 10.: Photo from a visit to the CERN IRRAD facility. SHUTTLE IRRAD-1.

Table 1: Irradiated samples investigated in this work.

Type	Sensor name	Fluence (p/cm^2)
High fluence irradiation		
n-LGAD {1}	R16375_W1_51015_nLGAD	1×10^{13}
	R16375_W1_51019_nLGAD*	4×10^{14}
	R16375_W1_51042_nLGAD	8×10^{14}
	R16375_W1_51044_nLGAD	1.5×10^{15}
	R16375_W1_51058_nLGAD	2.5×10^{15}
n-PiN {1}	R16375_W4_51004_PiN	1×10^{13}
	R16375_W4_51043_PiN*	4×10^{14}
	R16375_W4_51044_PiN	8×10^{14}
	R16375_W4_51082_PiN	1.5×10^{15}
	R16375_W4_51083_PiN	2.5×10^{15}
Step-by-step irradiation		
n-LGAD {2}	R16375_W1_LG04_nLGAD*	1×10^{12} 2×10^{12} 4×10^{12} 6×10^{12} 8×10^{12} 1×10^{13}
n-PiN {2}	R16375_W1_LG16_PiN*	

* - samples were annealed
{1} – samples without a window opening on metal (smaller active area)
{2} – samples with a window opening on metal (bigger active area)

Later for TCT measurements a selected subset of samples was glued and wire bonded to customized printed circuit boards (PCBs) with conductive silver glue (see *Fig. 11* and *Fig. 12*).

For edge-TCT measurements one edge of the sample without opening (because the common top TCT measurement would not be possible with this due to the metal) was polished with sandpaper with a very fine grit and diamond paste. A polished edge reduces the likelihood of signal artifacts caused by scattering or reflections of the laser beam at the sensor's edge.

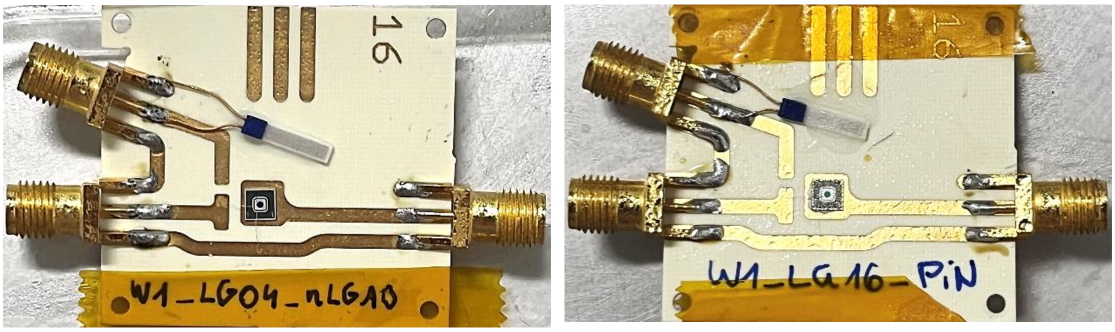

Fig. 11.: Step-by-step irradiated samples: n-LGAD (left) and n-PiN (right) with a window opening on metal (fluence $1{\times}10^{13}$ p/cm^2) bonded on PCB for TCT with UV measurements.

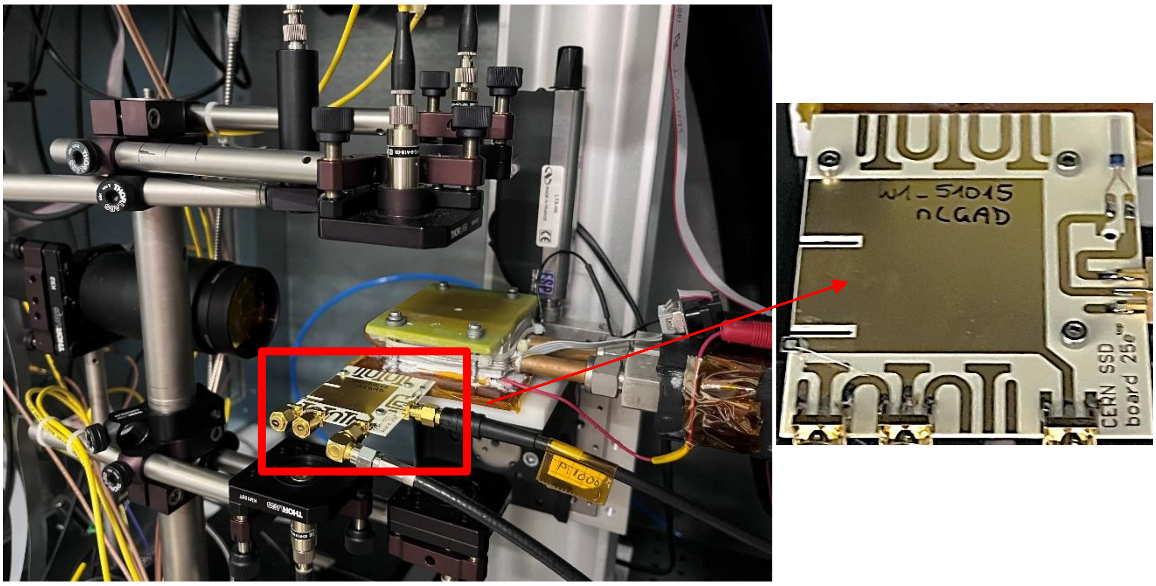

Fig. 12.: High fluence irradiation sample without a window opening on metal ($1{\times}10^{13}$ p/cm^2) bonded on PCB for edge-TCT with IR measurements.

3 EXPERIMENTAL SETUP

3.1 I-V/C-V MEASUREMENTS

For characterizing the leakage current and capacitance, the I-V/C-V probe station at the SSD lab (28/2-019) was used for the measurements presented in this work (see *Fig. 13*).

The list of measurement devices the probe station is composed of:

- Cooling Unit P100
- LCR Meter (Agilent E4980)
- High-Voltage Source (Keithley 2410)
- SourceMeter (Keithley 2410)
- Picoammeter (Keithley 6487)

For performing a measurement, the sensors are placed on a temperature-controlled chuck, where they are fixed with vacuum. Micro-meter needles and the chuck are used to establish the electrical connection (*Fig. 13*). The chuck and needles are enclosed with a removable lid during the measurements to prevent light exposure of the sensor [4]. If the sensor is cooled, the enclosure is flushed with dry air to avoid condensation. Bias voltage to the sensor is provided with a Keithley 2410 power supply (*Fig. 14*). The pad current is measured with a Keithley 6487 picoammeter. For measurements of the capacitance, a LCR Meter Agilent E4980 is used. A CV/IV custom-built switch box is used to change the setup configuration between both I-V and C-V modes. A small AC signal is superimposed on the DC bias. The AC signal induces a small charge variation in the device, which corresponds to the capacitance [4]. The LCR meter measures the impedance.

Fig. 13.: Photos of I-V/C-V probe station.

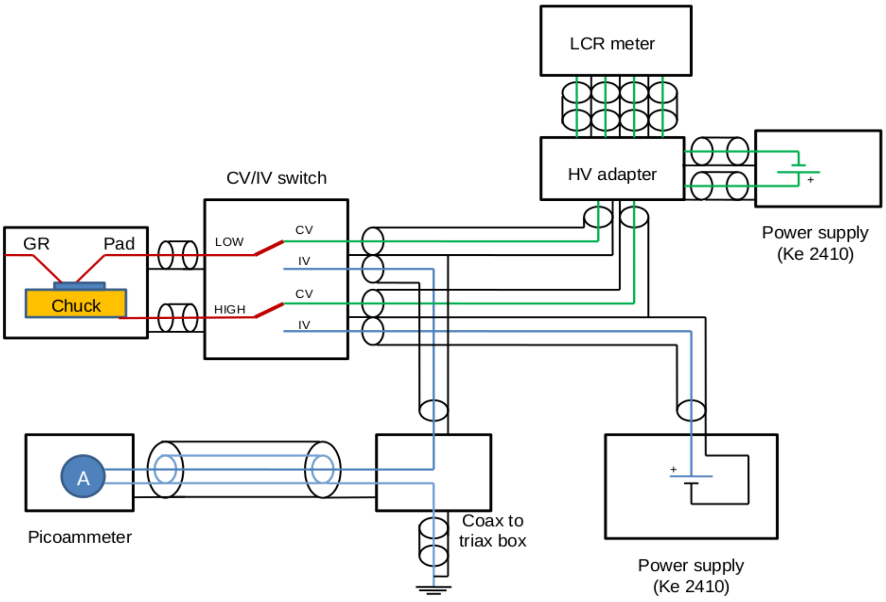

Fig. 14.: Electrical setup of the IV/CV probe station [9].

3.2 TCT MEASUREMENTS

The Transient Current Technique (TCT) is based on the analysis of the current induced by the movement of charge carriers inside a sensor when irradiated with a picosecond pulsed laser (see *Fig. 15* and *Fig. 16*). The sensor on a PCB is mounted on a copper plate, the temperature of which can be regulated by means of a Peltier element connected to a Temperature Controller, allowing to perform the measurement at controlled temperature in a range from -20°C to 30°C (*Fig. 17*). A chiller unit is responsible for the circulation of refrigerating liquid through the warm part of the Peltier. In order to move the sensor on PCB under the laser spot, the cooling plate is mounted on a 3-axis motorized linear stage system [9] (*Fig. 17*).

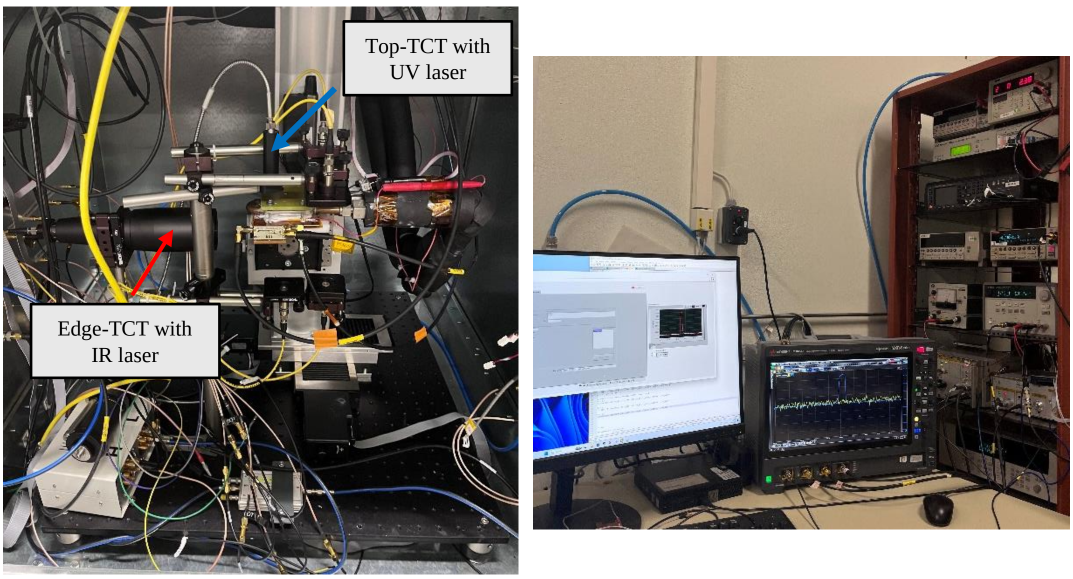

Fig. 15.: Photos of top-TCT/edge-TCT measurement system.

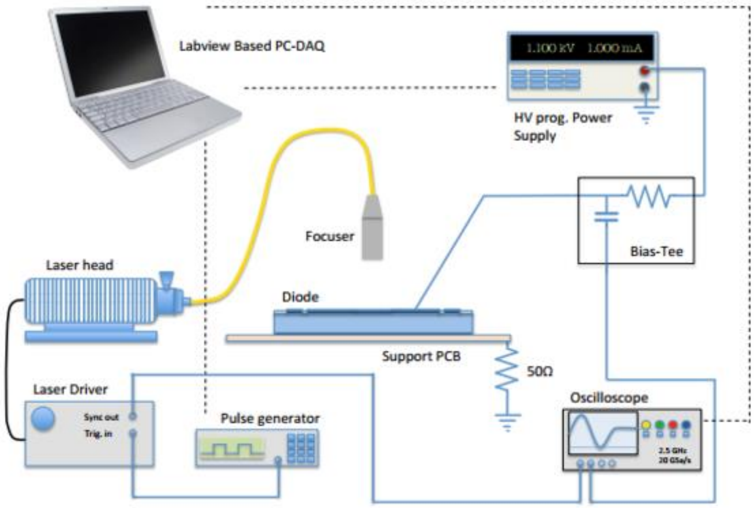

Fig. 16.: Simplified schematic of front TCT setup [9].

The setup features 6 different combinations of wavelength and illumination directions (*Fig. 18*): red laser (660 nm) with top and bottom illumination; IR laser (1064 nm) with top, bottom and edge (e-TCT) illumination; UV laser (nm) with top illumination [9].

A CIVIDEC C2-HV current amplifier (2 GHz) converts the generated current pulse into a voltage signal, which is visualized and recorded using Agilent DSO9254A oscilloscope. A bias tee is integrated in the sensor enclosure to decouple the DC bias voltage provided by an external High Voltage Supply (HVPS) from AC signal that needs to flow towards the amplifier [9].

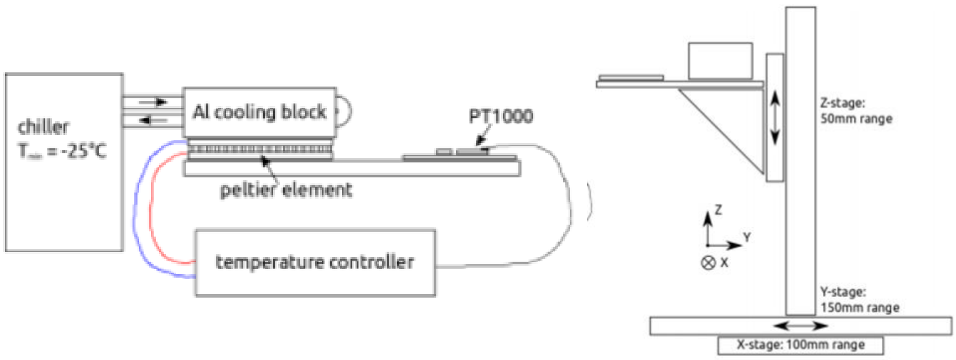

Fig. 17.: Schematic of the cooling system (left) and the linear stage system (right) for TCT [9].

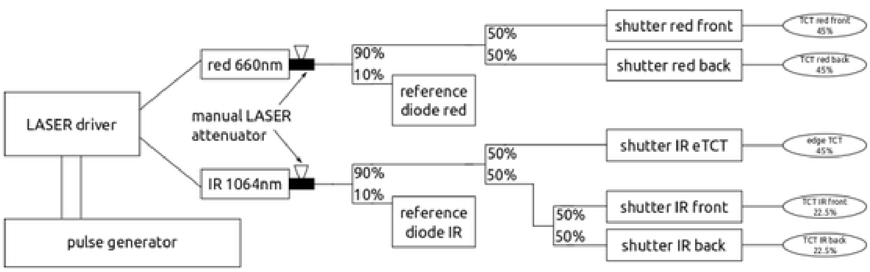

Fig. 18.: Schematic of the optical system for TCT [9].

4 ELECTRICAL CHARACTERIZATION

4.1 C-V AND I-V MEASUREMENTS AND ANNEALING FOR HIGH FLUENCE IRRADIATION SAMPLES

In this work C-V characteristics were measured for samples with high irradiation fluences, and measurements were performed at -20°C and for 1 kHz frequency. As can be seen from *Fig.19*, only one n-LGAD sample with the lowest irradiation fluence ($\Phi = 1\times10^{13}$ p/cm^2) shows similar to LGAD behaviour recognizable by the peak (around 40 V), indicating gain layer depletion voltage. In addition, there is no systematic change of capacitance for n-LGADs in comparison to PiNs (capacitance increases with irradiation fluence). Before irradiation, as could be seen from *Fig. 20*, the gain layer depletion voltage of n-LGADs was between 25 V and 30 V.

The irradiation fluences were chosen based on the typical values for studying irradiation damage in p-type LGADs. Presumably, due to different effects as type inversion in n-type material which creates inhomogeneous electric fields, the observation of changes in the gain layer (shift of gain layer depletion voltage) proved to be comparatively more difficult than for the commonly studied p-type LGADs.

In addition to this, it was found that measurements of the leakage current of the devices, which differ by approximately 20% for repeated measurements and do not consistently match one another for higher irradiation fluence (*Fig. 24*). The question of measurement reproducibility and setup reliability arose, which was investigated using different measurement configurations such as IV/CV measurements with and without vacuum, changing position of the sample on temperature-controlled chuck, etc. These results will be discussed later in this work.

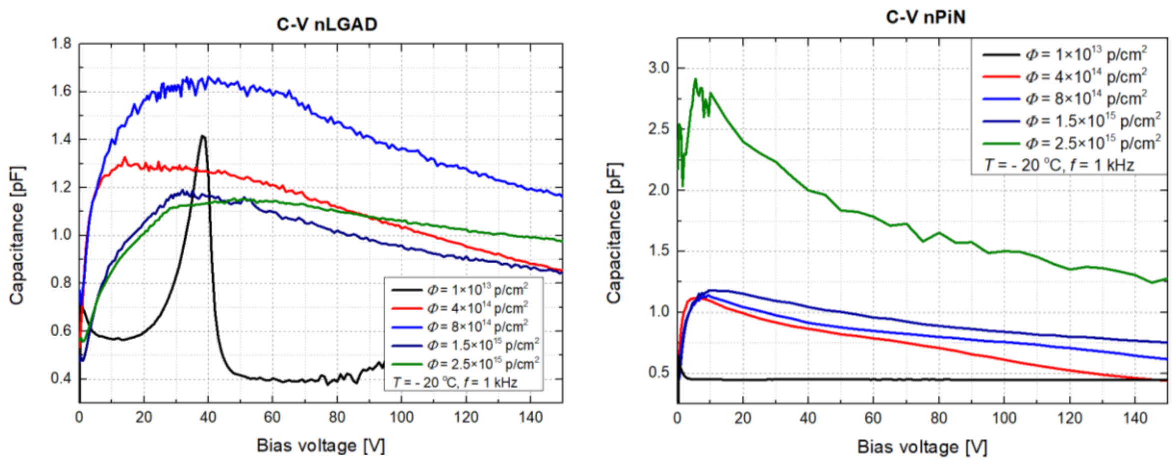

Fig. 19.: C-V measurements for n-LGADs (left) and n-PiNs (right) (without window opening on metal) irradiated with different fluences. Measurements performed at -20°C and for 1 kHz frequency.

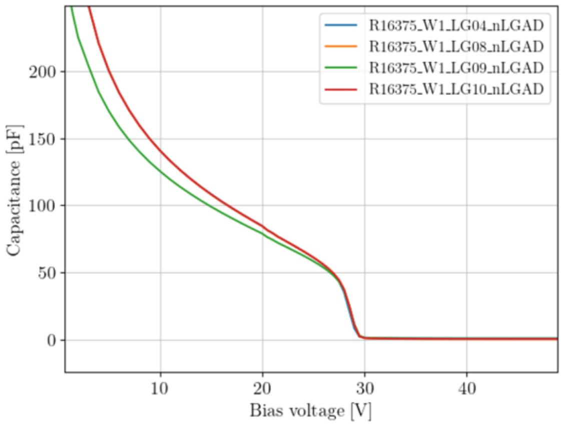

Fig. 20.: C-V measurements for n-LGADs implemented before irradiation [5].

In order to examine the influence that the proton irradiation has on the leakage current of the sensors, I-V characteristics of the samples were measured and are presented in *Fig. 21* (measurements performed at -20°C). The ample with the lowest irradiation fluence shows similar to LGAD behaviour with a breakdown voltage at around 120 V. Before irradiation, breakdown of n-LGADs starts at around 200 V (see *Fig. 22*). For other higher fluences (from 8×10^{14} p/cm^2) leakage current is very similar to each other, and behaviour is comparable to PiNs.

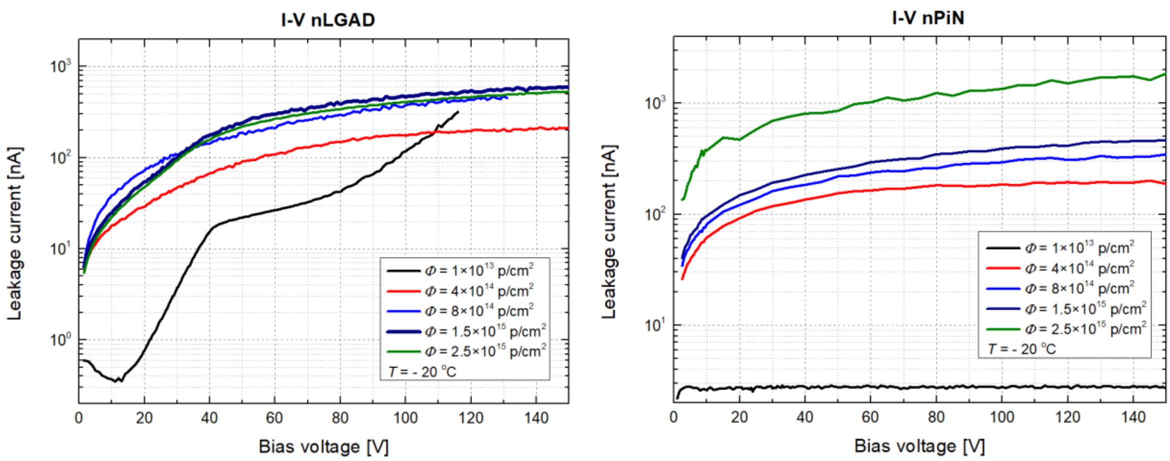

Fig. 21.: I-V measurements for n-LGADs (left) and n-PiNs (right) irradiated with different fluences.

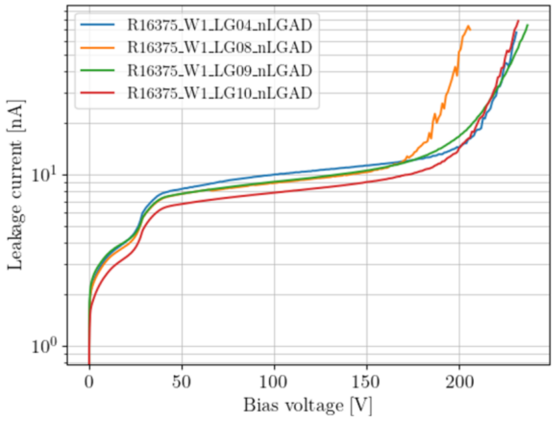

Fig. 22.: I-V measurements for n-LGADs performed before irradiation [5].

An isochronal annealing starting from 60°C up to 120°C (with 20°C temperature steps) for n-LGAD and 100°C for n-PiN for 20 minutes each was carried out for the 4×10^{14} p/cm^2 sample to examine the temperature effect on the leakage current. The aim is to inquire if it is possible to recover some of the LGAD like behaviour (see *Fig. 22*). The annealing temperature shall not be confused with the measurement temperature of the leakage current. The mechanisms leading to annealing of defects can be divided in migration, formation and dissociation processes:

- Migration and complex formation. The defects become mobile at certain temperature. They migrate through the silicon lattice until they are gathered at sinks (surface, dislocations, etc.), recombine with their counterparts or form new defects by association with identical or other types of defects (or impurities) [10].
- Dissociation. A complex (defect composed of more than one constituent) dissociates into its components if the lattice vibrational energy is sufficient to overcome the binding energy. At least one of the constituents migrates through the lattice until it forms another defect or disappears into a sink [10].

As could be seen from *Fig. 22 and Fig. 23*, annealing effect does not show any systematic changes of the leakage current and capacitance with increasing temperature.

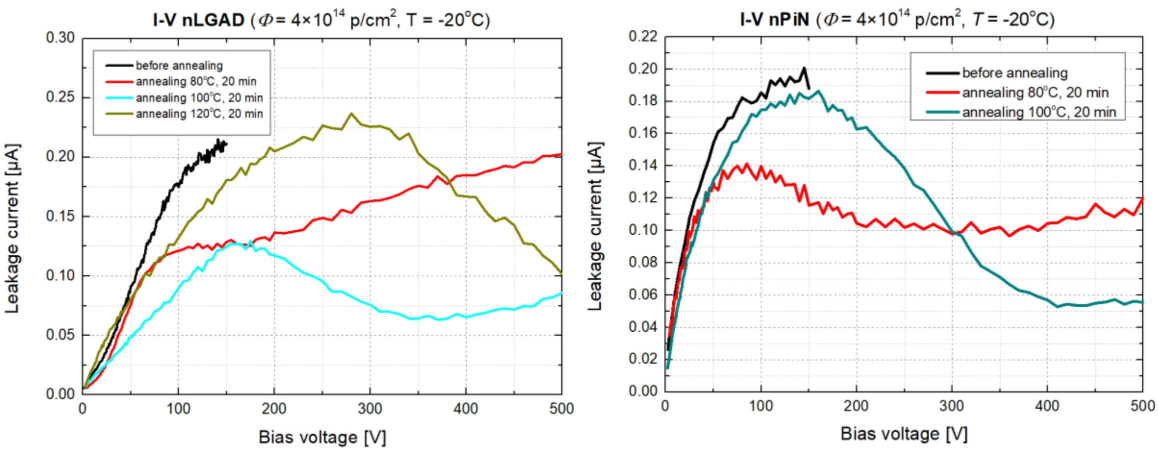

Fig. 22.: I-V measurements before and after annealing procedure for n-LGADs (left) and n-PiNs (right) irradiated with the same fluence of 4×10^{14} p/cm^2.

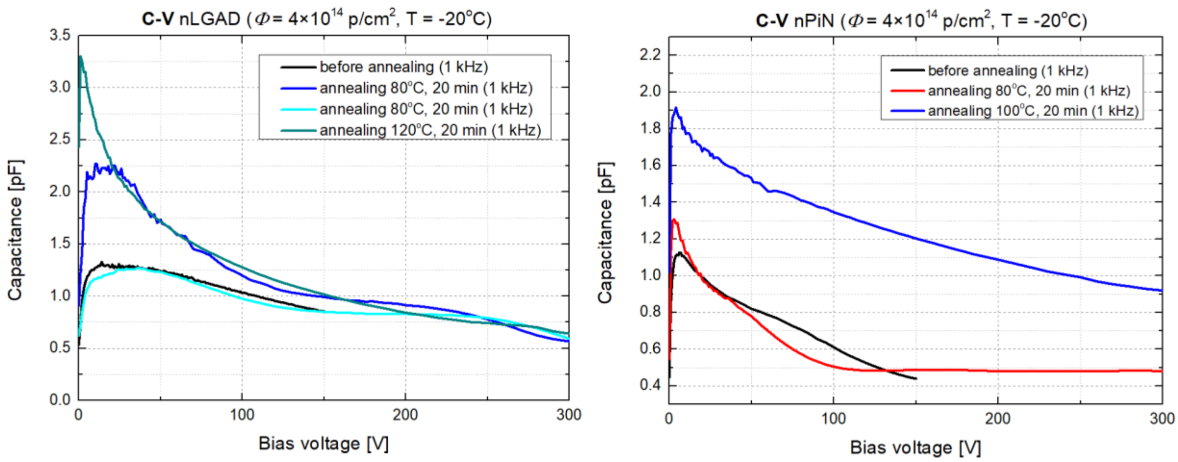

Fig. 23.: C-V measurements before and after annealing procedure for n-LGADs (left) and n-PiNs (right) irradiated with the same fluence of 4×10^{14} p/cm^2.

Mentioned above measurement reproducibility tests showed that there is no problem with a setup. Ramp up and down hysteresis (*Fig. 25*) looks similar (without the 20% change for individual measurements of the same sample (see *Fig. 24*)) and the difference of the leakage current values (about 20%) for distinct measurement configurations presumably might be explained by the small size of an active area of the samples and resulting stability problems of the placement with the vacuum. Blue and orange curves represent the same measurement under the same conditions but with a ~20% difference in leakage current (*Fig. 24*).

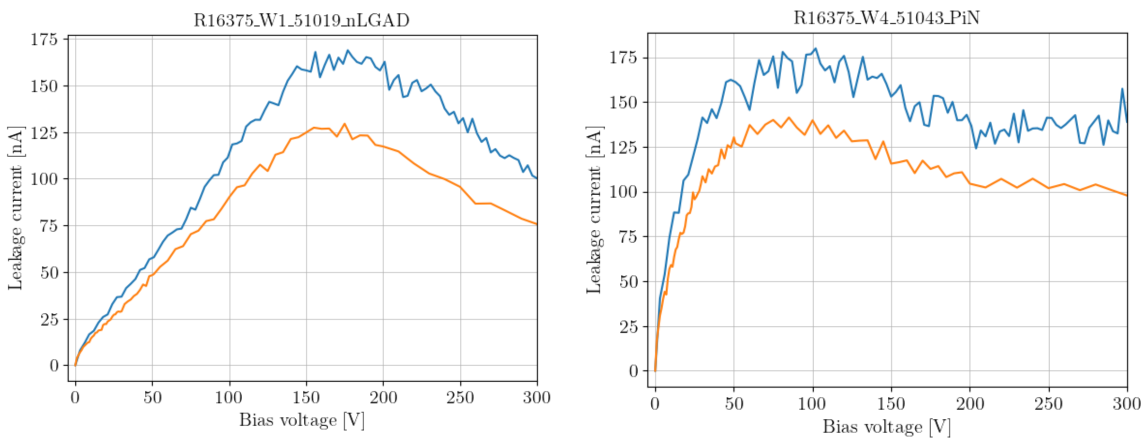

Fig. 24.: Reproducibility tests of the measurements for n-LGAD (left) and n-PiN (right) irradiated with fluence of 4×10^{14} p/cm^2. Measurements performed at -20°C.

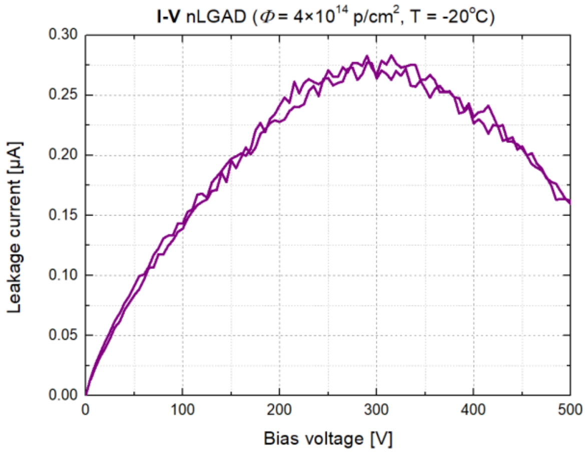

Fig. 25.: Hysteresis: ramp up and down for sample irradiated with fluence of 4×10^{14} p/cm^2.

4.2 C-V AND I-V MEASUREMENTS FOR STEP-BY-STEP IRRADIATION SAMPLES

As previous samples irradiated with higher fluences showed inconclusive results regarding the effect of irradiation on the bulk and gain layer, the decision was made to irradiate one n-LGAD and one n-PiN for comparison step-by-step with lower fluences up to 1×10^{13} p/cm^2. Measurements were performed at 20°C and -20°C with annealing at 80°C for 4 min after each irradiation step to compensate for uncertainties with potential annealing at room temperature and to make the results more comparable. For step-by-step irradiation we observe a decrease of capacitance with increasing irradiation fluence at 20°C and for n-PiNs temperature differences did not significantly change C-V curves (*Fig. 26*). Peak appearance could be noticed at -20°C for all following fluences (*Fig. 27*). In addition to this, the peak is also strongly dependent on the frequency (see *Fig. 30*, *section 4.3*).

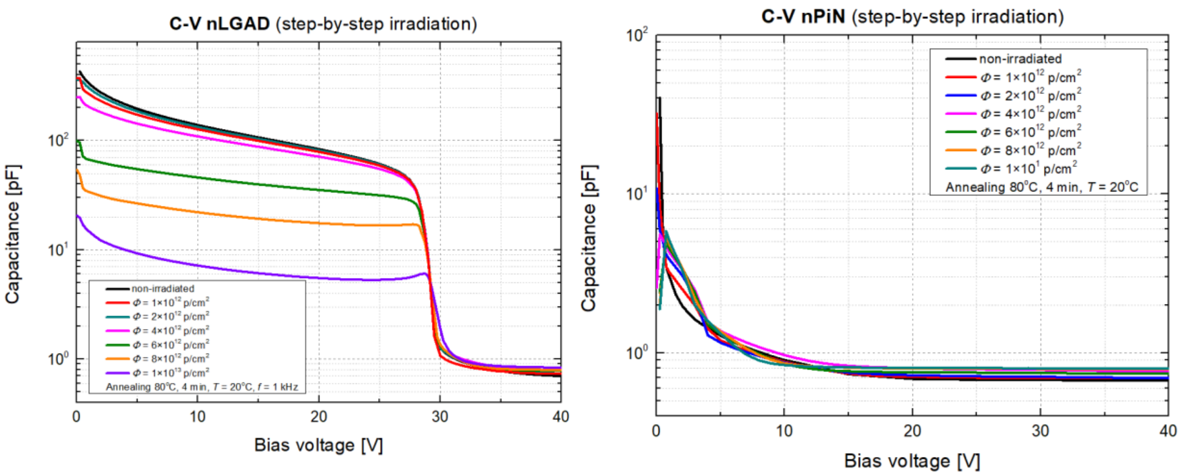

Fig. 26.: C-V measurements for n-LGAD (left) and n-PiN (right) irradiated step-by-step with different fluences at 20°C and 1 kHz frequency.

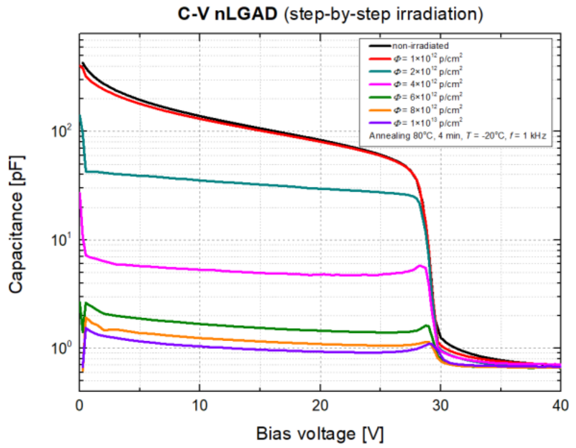

Fig. 27.: C-V measurements for n-LGAD at -20°C and 1 kHz frequency (left) and comparison of the same step-by-step irradiated sample with fluence of 4×10^{12} p/cm^2 at 20°C and -20°C, and 1 kHz frequency (right).

For I-V systematic increase of leakage current was observed for both n-LGADs and n-PiNs (*Fig. 28*). Also, for n-LGAD and n-PiN noticeable systematic effect of annealing: leakage current is decreasing with annealing after each irradiation step. At a bias voltage of 150 V, the leakage current extracted from the I-V curves as a function of irradiation fluence for both n-the LGAD and n-PiN is roughly linear with different slopes, as the gain influences the leakage current increase of LGAD differently as for the PiN. For n-LGADs no strong shift of gain layer depletion voltage was observed. Comparison of leakage current as a function of irradiation fluence for n-LGAD and n-PiN is presented in *Fig. 29*.

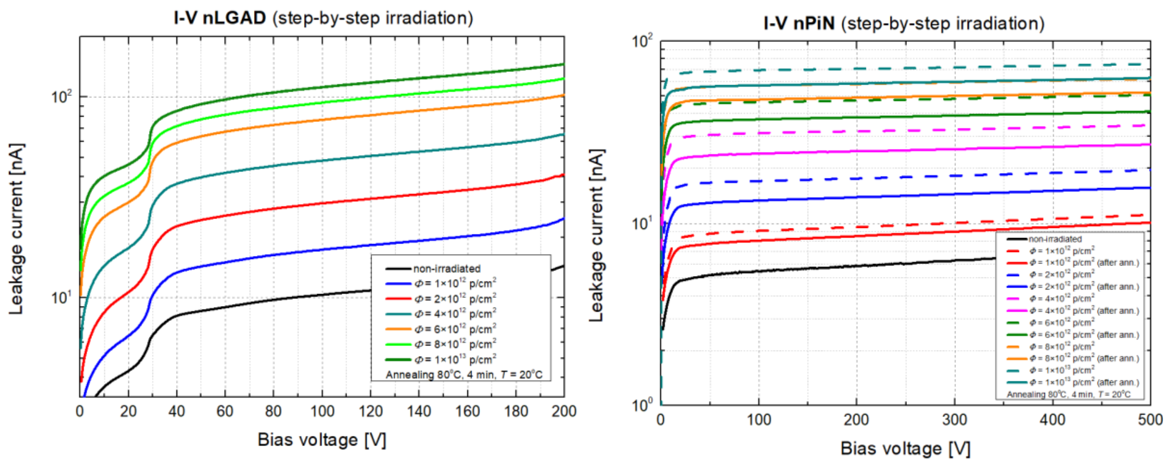

Fig. 28.: I-V measurements for n-LGAD (left) and n-PiN (right) irradiated step-by-step with different fluences at 20°C.

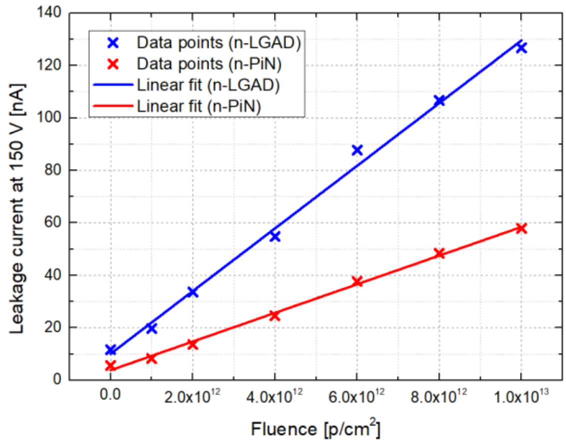

Fig. 29.: Comparison of the leakage current as a function of irradiation fluence at bias voltage of 150 V for n-LGAD and n-PiN. Measurements performed at 20°C.

4.3 Frequency dependence

Frequency dependent C-V measurements were also performed, and results show a different position of the gain layer depletion voltage related peak for two different types of the sensors with and without opening (see *Table 1*) irradiated with the same fluence of 1×10^{13} p/cm^2. The tendency of decreasing capacitance with increasing frequency stays the same for both samples (*Fig. 30*). Gain layer depletion voltage before irradiation for both samples with and without opening on metal was around 30 V. No gain layer depletion voltage shift for step-by-step irradiated sample compared to the other measured sample from high fluence irradiation campaign with a shift towards higher values (shift from 30 V to 40 V), contrary to expectations of a shift to lower values with potential damage to the gain layer. This difference could originate from different annealing.

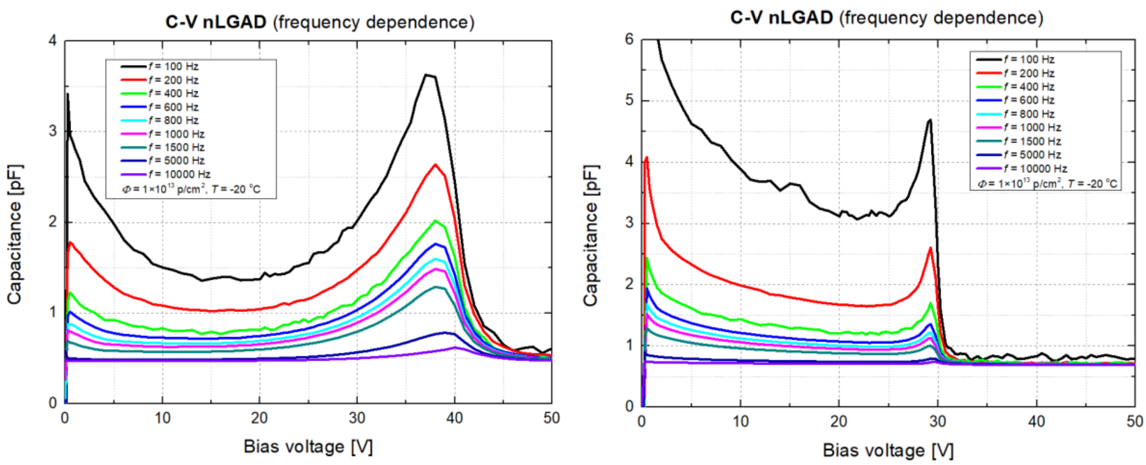

Fig. 30.: C-V measurements with different frequencies for high fluence irradiated sample (left) and step-by-step irradiated sample (right) with the same irradiation fluence of 1×10^{13} p/cm^2.

4.4 TEMPERATURE DEPENDENCE

Temperature dependent I-V for the same step-by-step irradiated sample after irradiation showed similar behaviour as before irradiation. Breakdown voltage shifted to lower bias voltages due to impact ionization in a gain layer, as was expected (*Fig. 31*). Gain layer depletion voltage is approximately the same (around 30 V).

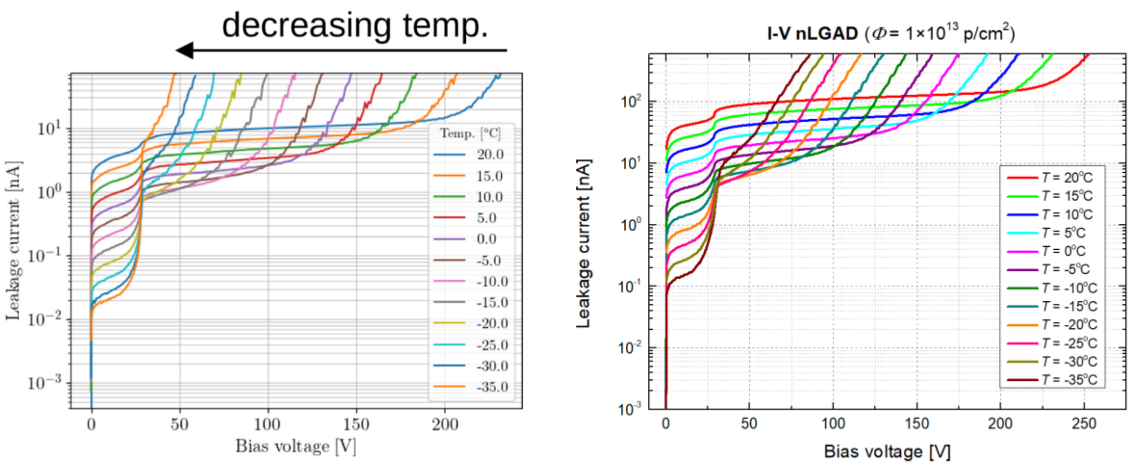

Fig. 31.: I-V measurements with different temperatures for the same sample before and after irradiation (1×10^{13} p/cm^2).

5 LASER CHARACTERIZATION

5.1 TCT MEASUREMENTS WITH UV LASER FOR STEP-BY-STEP IRRADIATED SAMPLE

TCT measurements are based on the analysis of the transient current pulse from the drift of charge carriers in the electric field inside a biased sensor. Charge injection is possible with the use of pulsed laser source. TCT measurements with UV laser (375 nm) were performed for one n-type LGAD and one PiN with opening irradiated with fluence of $1{\times}10^{13}$ p/cm^2. X-Y scan for both n-LGAD and n-PiN was done to find a center of the opening window (*Fig. 32*).

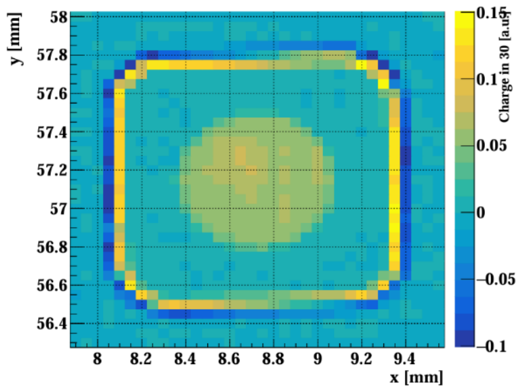

Fig. 32.: X-Y scan for n-PiN. Different colours refer to collected charge in 30 s. Yellow colour represents larger collected charge in the sensor.

As could be seen from the graph (*Fig. 33*), collected charge is increasing with higher laser intensity. Observed step in the collected charge for n-PiN could be interpreted as a systematic effect arising from the sample and connected to increasing intensity (*Fig. 33*).

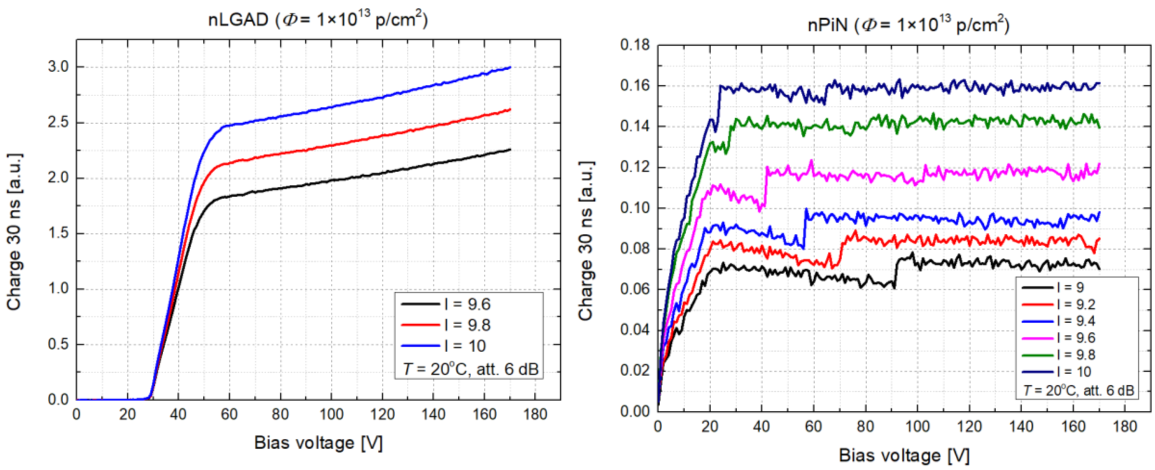

Fig. 33.: Collected charge with different laser intensities for n-LGAD (left) and n-PiN (right) after irradiation.

Measurements were performed at 20°C using highest laser intensity I = 10 and attenuator 6 dB. Gain of n-LGAD is calculated as Q_{nLGAD}/Q_{nPiN}, e.g., ratio of collected charge in n-LGAD and charge fitted from n-PiN (constant value) (*Fig. 34*).

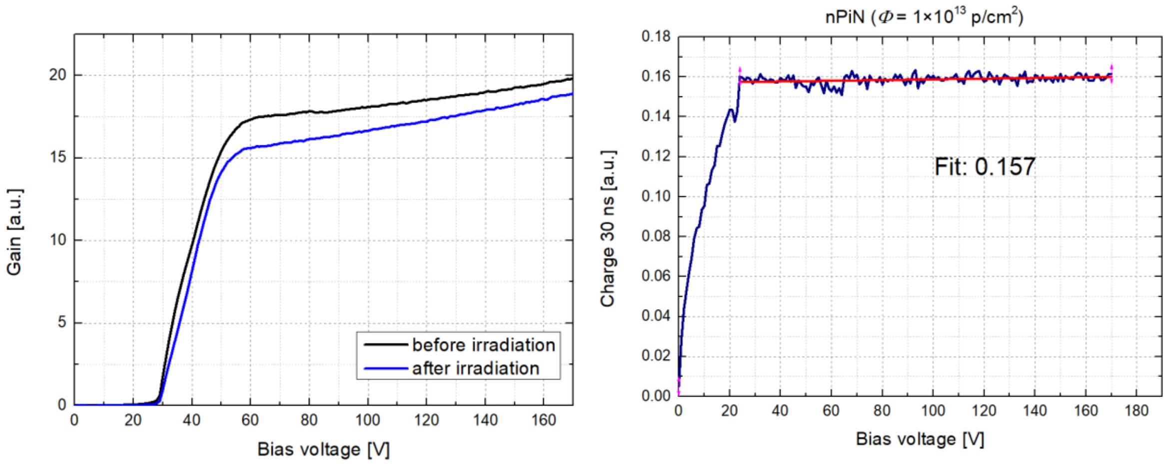

Fig. 34.: Comparison of n-LGAD gain before and after irradiation (1×10^{13} p/cm^2) (left) and charge fitted from corresponding n-PiN measurement (after irradiation) (right).

5.2 Edge-TCT measurements with IR laser for step-by-step irradiated sample

Infrared light (1064 nm) can be injected from one edge into the sample to probe the sensor response as a function of depth in the bulk. Edge-TCT is implemented to get an impression of the shape of the electric field. Edge-TCT measurement shows contributions from both electron and hole drift along sensor thickness and can give indications for the electric field distribution. The charge is calculated as the integral of a waveform (*Fig. 35*) starting at the injection time of the pulse (the same procedure as in UV TCT with recorded waveforms).

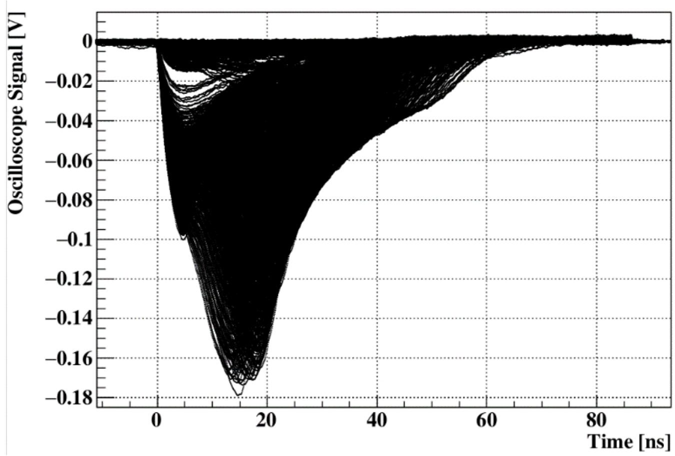

Fig. 35.: Waveforms measured after full depletion of the sensor (>50 V).

In order to investigate the distribution of electric field along z-axis for n-type LGAD without a window opening on metal, a Z-X scan was performed to find the beam waist and ensure a good IR laser focus point for the further edge-TCT measurements (*Fig. 36*).

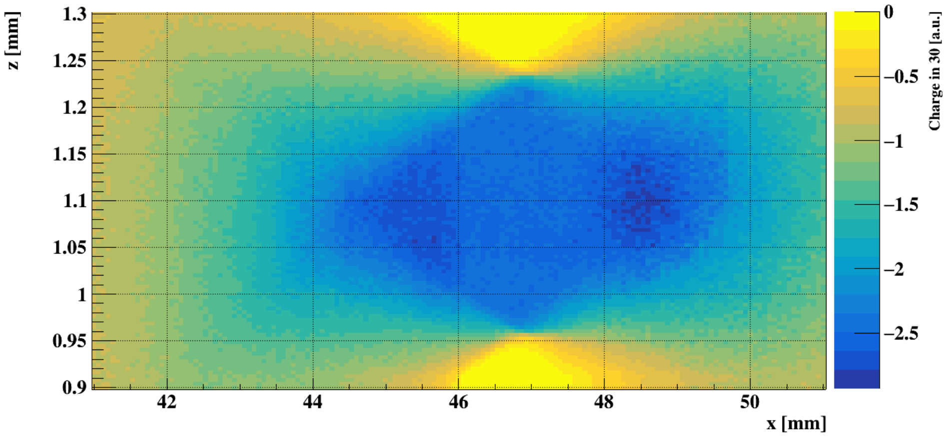

Fig. 36.: Z-X scan to determine beam waist for further edge-TCT measurements.

Prompt current measurements after 600 ps as a function of position along sample's depth for different bias voltages (*Fig. 37*) show that drift velocity increases with the bias voltage. As could be seen from the graph, roughly flat plateau of the curves indicates that there is no visible double junction effect in the sample. Fluctuations from flat plateau may come from inaccurate polishing of the small edge of the sensor.

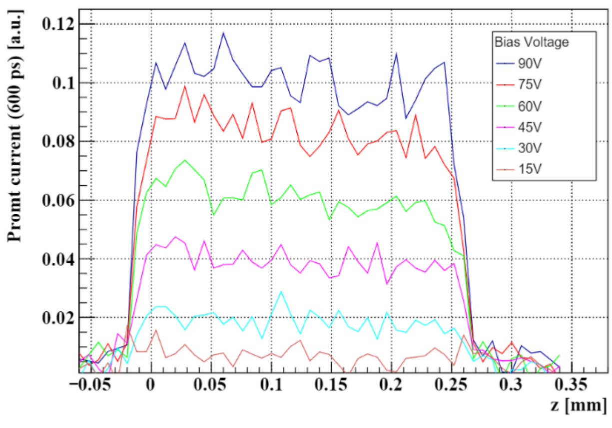

Fig. 37.: Prompt current after 600 ps as a function of position along sample's depth for different bias voltages (*high irradiation* sample without opening irradiated with fluence of $1{\times}10^{13}$ p/cm^2). Measurements implemented at -20°C.

6 CONCLUSIONS

In this study, the effects of proton irradiation on n-type LGADs through two distinct irradiation campaigns were investigated: one involving high fluences (for samples without opening) and the other employing a step-by-step irradiation approach (for samples with opening).

Our results indicate that the gain layer depletion voltage does not exhibit a noticeable shift for the step-by-step irradiated samples up to a fluence of 1×10^{13} p/cm^2. In contrast, the sample subjected to 1×10^{13} p/cm^2 from the higher fluence irradiation shows a shift of the gain layer depletion voltage towards higher values, which could be attributed to different annealing effects. All other samples from 4×10^{14} p/cm^2 to 2.5×10^{15} p/cm^2 (which are typical values for irradiation campaigns with p-type LGADs) are not fully understood yet, however, show no distinct gain layer depletion behaviour from which one could conclude on the degradation of the gain layer with irradiation. The temperature dependence of the impact ionization behaviour in n-type LGADs was found to be consistent with expectations of linearity from in HEP p-type LGADs. In addition to this, the frequency dependence of C-V measurement is comparable between similar samples of the two irradiation campaigns. However, our irradiation experiments suggest that donor removal in the gain layer is less easily observed compared to acceptor removal, possibly due to type inversion in the n-bulk.

Top-TCT measurements with UV light were carried out for the purpose of studying how collected charge is related to different laser intensities and compare n-LGAD gain before and after irradiation. The collected charge is increasing with higher laser intensity and gain is reduced after irradiation. Edge-TCT measurements with IR light were conducted in order to measure the shape and the distribution of the electric field along z-axis for n-type LGAD without a window opening on metal. A z-x scan was performed to find the beam waist and ensure a good IR laser focus point as well as prompt current measurements after 600 ps as a function of position along sample's depth for different bias voltages. Drift velocity increases with the bias voltage. Fluctuations from a flat plateau may come from inaccurate polishing of the small edge of the sensor. No clear evidence of a double junction could be found from these initial measurements; further samples are to be investigated in this respect.

Despite some challenges and difficulties in interpreting the results, valuable insights were gained. These initial measurements allowed us to formulate hypotheses about the behaviour of the sensors under irradiation. Based on these findings, several ideas and proposals for future measurement campaigns have been developed to further investigate open questions, such as the potential presence of double junctions and the donor removal process.

Further investigations are required to fully understand the impact of high irradiation fluences on n-type LGADs. Specifically, we plan to conduct additional edge-TCT measurements on samples subjected to higher irradiation fluences to probe the potential existence of double junctions. Additionally, neutron irradiation studies are planned to further examine the donor removal process, which could provide critical insights into the radiation hardness of these devices as well as for HEP LGAD concepts.

7 REFERENCES

1. M. Moll et al., *Introduction to Silicon Detectors for the LHC and Radiation Damage to Silicon Detectors*. Lab Training Session: Solid State Detectors. ESIPAP School – 2023. Internet access: https://indico.cern.ch/event/1064512/contributions/4628386/attachments/2355766/4054938/220128-ESIPAP-Silicon-Detectors-INTRO.pdf.
2. M. Moll, *Displacement Damage in Silicon Detectors for High Energy Physics*. IEEE Transactions on Nuclear Science, Vol. 65, No. 8, August 2018. DOI:10.1109/TNS.2018.2819506.
3. G. Lindstrom et al., *Radiation hardness of silicon detectors — a challenge from high-energy physics*. Nuclear Instruments and Methods in Physics Research A 426 (1999) 1—15. Internet access: https://doi.org/10.1016/S0168-9002(98)01462-4.
4. M. Wiehe, *Development of a Two-Photon Absorption - TCT system and Study of Radiation Damage in Silicon Detectors*. PhD Dissertation. Albert-Ludwigs-Universität Freiburg im Breisgau, 2021. Internet access: https://cds.cern.ch/record/2795933/?ln=ca.
5. V. Kraus et al., *1st DRD3 week, WG2, 18th of June* (presentation). Internet access: https://indico.cern.ch/event/1402825/contributions/5999052/attachments/2879317/5044420/Veronika_Kraus_DRD3_LGAD_Irrad_nLGADs.pdf.
6. M. Moll, *Acceptor removal - Displacement damage effects involving the shallow acceptor doping of p-type silicon device*. The 28th International Workshop on Vertex Detectors- Vertex2019. DOI:10.22323/1.373.0027.
7. J. Villegas et al., *Gain measurements on NLGAD detectors.* Nuclear Inst. And Methods in Physics Research, A 1055 (2023) 168377. Internet access: https://doi.org/10.1016/j.nima.2023.168377.
8. V. Sola et al., *A compensated design of the LGAD gain layer*. Nuclear Inst. And Methods in Physics Research, A 1040 (2022) 167232. Internet access: https://doi.org/10.1016/j.nima.2022.167232.
9. SSD Setups – Twiki – CERN. Internet access: https://twiki.cern.ch/twiki/bin/view/SolidStateDetectors/SolidStateDetectorsSetups.
10. M. Moll, *Radiation damage in silicon particle detectors – microscopic and macroscopic properties*. Dissertation. Fachbereichs Physik der Universitat Hamburg, 1999. Internet access: https://mmoll.web.cern.ch/thesis/.